ELASTIC AND RAMAN LIDAR SOUNDING OF COASTAL WATERS. THEORY, COMPUTER SIMULATION, INVERSION POSSIBILITIES

Eleonora Zege, Iosif Katsev, Alexander Prikhach and Alexey Malinka

B. I. Stepanov Institute of Physics, National Academy of Science of Belarus,
220072 Minsk, Belarus; eleonor(at)zege.bas-net.by

ABSTRACT

This paper outlines the software AOLS (Airborne Oceanic Lidar Simulator) for quasi real-time computer simulation of airborne oceanic lidar performance and the underlying semi-analytical theory of a lidar return with multiple scattering. The model provides the signal in elastic lidar with polarization devices and with Raman and fluorescence channels. The model data compare exceptionally well with experimental data provided as a result of the HyCODE 2001 field test. The presented modelling is a powerful tool not only to predict and to optimise the performance of oceanic airborne lidar but also to develop and verify retrieval techniques. An analytical inversion of the lidar equation with multiple scattering and the first advances in the inversion of lidar profiles with multiple scattering are presented.

Keywords: Ocean lidar sounding, inverse problem, computer simulation, multiple scattering

INTRODUCTION

The concept of airborne oceanic lidar for ocean survey, including sea bottom detection and bathymetry and water column characterization, was recognized in the 1960ies (1,2). Since that time airborne laser bathymetry has become “an established operational technique, which has been proven to be an accurate, efficient, cost-effective, safe, and flexible method for rapidly charting near-shore waters, adjacent beaches, and coastal engineering structures” (see the detailed review (3) and references in it). Nevertheless, in spite of lidar bathometers provide lidar waveforms that carry information of the seawater Inherent Optical Parameters (IOP) profiles, the only averaged diffuse attenuation coefficient has sometimes been estimated from measured lidar waveforms (4). The lack of an adequate theory of the problem and the lacking direct relationships between lidar return and optical characteristics of seawater are the main obstacles on the way to make lidar sounding the quantitative exploring method for seawater optical characteristics measurements. As it was shown (see, for instance, (5,6)), including multiple scattering is of prime importance in such a theory.

In this paper we generalize the semi-analytical theory of lidar return with multiple scattering developed by the authors (7-11) in one comprehensive general approach. This approach summarizes the analytical theories of the elastic (7,8) and Raman (11) lidar returns with and without polarization (9,10) and additionally includes the laser-induced fluorescence. The developed solutions, which include multiple scattering and directly relate the lidar signals to the vertical profiles of the IOP of the ocean water, form the core of the algorithm for a quasi real-time computer simulation of airborne oceanic lidar performance.

This paper outlines the family of software AOLS (Airborne Oceanic Lidar Simulator). Different members of the AOLS family simulate the performance of the various mono- and bi-static lidar systems, launched either on a vehicle in air or on an underwater vehicle, with or without polarization devices, with or without Raman or fluorescence channels.

The software AOLS is a powerful tool to

- predict the performance of oceanic airborne lidars;
- optimize the lidar design for a given mission;

- estimate the efficiency of new lidar designs and techniques without or before developing a hardware;
- develop and verify various retrieval techniques including coupling multispectral elastic and non-elastic lidar returns.

This software may be used for further improving lidar bathymetry instruments (both hardware and waveform processing algorithms) with the goal to meet the accuracy standards generally accepted for hydrography and established by the International Hydrographic Organization (12). In this paper we derive a new solution of the lidar equation with multiple scattering and demonstrate how coupling of this solution with the developed fast simulation provides the basis for lidar waveform inversion. One more idea of the retrieval of seawater scattering profiles using a laser with two specified wavelengths, and the elastic and Raman channel signal return is outlined.

METHODS

Simulation of oceanic airborne lidar performance

The computer simulation is the fastest and cheapest way to answer many questions, which arise while solving the problem of seawaters monitoring. The developed theory of the lidar return from stratified seawater was used to design an efficient quasi-real time algorithm simulating the performance of various airborne oceanic lidars.

We have recently developed a family of software AOLS, simulating lidar returns of airborne and underwater lidars with and without polarization devices, with and without water Raman channel and channel for laser-induced fluorescence. Any lidar design (including mono-static and bi-static lidars) as well as any characteristics of the laser and receiver are allowed to be taken for this modelling. Particular software simulating the performance of currently operating ocean lidars that are the K-meter Survey System (KSS) (4) and the Australian Laser Airborne Depth Sounder (LADS) system (13) were developed and tested.

Below we outline the basic software to simulate the performance of an oceanic lidar with elastic channel. The modelling of a channel with polarization devices, Raman channel and channel for registration of the laser-induced fluorescence has the same features as listed below.

While dealing with the problem of seawater lidar sounding from the air, a few specific features should be considered. In general, the power of the lidar return signal consists of the four terms:

$$F(t) = F_w(t) + F_{atm}(t) + F_{bot}(t) + F_{sur}(t) \quad (1)$$

where $F_w(t)$, $F_{atm}(t)$, $F_{bot}(t)$ and $F_{sur}(t)$ are the power of signal backscattering by seawater, atmosphere, seabed, and atmosphere-ocean interface, respectively. To compute the signal at the receiver input during daytime, the backscattering of sunlight is included as well.

The main term, which carries information about optical properties of seawater, is the component $F_w(t)$. The component $F_{sur}(t)$ contributes at small sounding depths and defines the minimal depth of the seawater lidar sounding. The atmospheric backscattering $F_{atm}(t)$ includes not only photons backscattered in the atmosphere on the way from a laser to a sea surface, but also the photons with the following history. The sea surface reflects the laser beam. A portion of these photons is backscattered by the atmosphere and reflected by the ocean surface toward a receiver. Sometimes this specific phenomenon restricts the range of water depths available for lidar sounding.

The following models of atmosphere, atmosphere-ocean interface, and seawater are used:

Atmosphere. The only parameter of the model is the meteorological visibility range at sea level.

Waves. Both smooth and rough sea surfaces can be treated. The basic wave spectral model of a wind-ruffled sea surface, which was suggested by R.E. Walker (14, p.264), is used with the wind speed V at the 10 m height above the sea level being the only surface roughness parameter.

Water. Water optical properties are assigned by depth profiles of the extinction and scattering coefficients, and the phase function $P(\beta)$. It is supposed that the phase function does not change with depth. Any available data may be included as input. For user convenience, for predictions and methodical studies a simple few-parameter model of the IOP of the homogeneous ocean (15) is included as optional. This model uses an empirical correlation between the single scattering albedo and extinction coefficient. To specify the homogeneous seawater parameters with this model is enough to include the extinction coefficient (or Secchi disc depth) and choose the phase function from the library.

The basic software provides:

- lidar return profiles from the ocean with different stratification;
- the components of the lidar return due to seawater, AOI, atmosphere, and sea bottom;
- the efficient coefficient of laser beam attenuation as a function of depth and its average value.

The software has the following features:

- real shape and duration of a laser pulse and an amplifier bandwidth of a receiver in a lidar system are regarded;
- forward pulse stretching is allowed for;
- both vertical and oblique observations sounding are allowable;
- all specific features of a real hydrosol phase function including those of the back scattering are allowed for;
- windy surface flash and the bottom return are included as well;
- the lidar return power is calculated with regard to backscattering enhancement due to the wave surface effect.

Effects of some of these features on the lidar waveforms were considered earlier. For instance, the regard to the shape and duration of a laser pulse and an amplifier bandwidth of a receiver and even the signal deconvolution were discussed in (16-18). The authors of papers (19,20) consider the effect of sea waves and light propagation on the lidar waveforms. The AOLS software allows all these features to be considered and estimated and also a lot of out-of-the-way effects, as pulse stretching, specific features of a real hydrosol phase functions including those in the near backward directions, backscattering enhancement due to the wave surface effect, and so on.

Figure 1 shows an example of a computer screen with all computed components in Equ. (1) of the lidar return. The software runs in an interactive mode on PC under *Windows*. It is user-friendly and presents many additional services and assistance functions. An experiment in the employment of the AOLS software by our group, groups from the USA (NAVIAIR) and the UK (DERA MALVERN) proved that it is a useful and convenient tool that saves a great deal of time and money.

Comparison of experimental and modelled data

A unique opportunity to directly compare profiles from the experimental LIDAR data and the model simulations was provided as a result of the HyCODE 2001 field test, where KSS Lidar profiles and near simultaneous *in situ* IOP profiles were collected off the coast of New Jersey. The KSS profiles were measured by the NAVIAR group. *In situ* data collected by Scott Pegau of the Ocean Optics Lab at the Oregon State University includes absorption and scattering profiles using WetLabs AC-9 instruments.

KSS (4) is a lidar with dual, independent receivers and a single transmitter. The transmitter is a 532 nm, short pulsed (7 ns), linearly polarized laser with computer adjustable energy output and manually adjustable beam divergence. During the HyCODE 2001 field test the KSS was configured without polarization elements and with a 3.5-inch square aperture plate which held a 532 nm interference filter with 4 nm bandwidth and neutral density filters for better daytime performance. The

tilt angle of the system was nominally set to 20° from nadir and the FOVs for receiver channels 1 and 2 were 10.7° and 4.3°, respectively. The transmitter divergence was set to 3.3°.

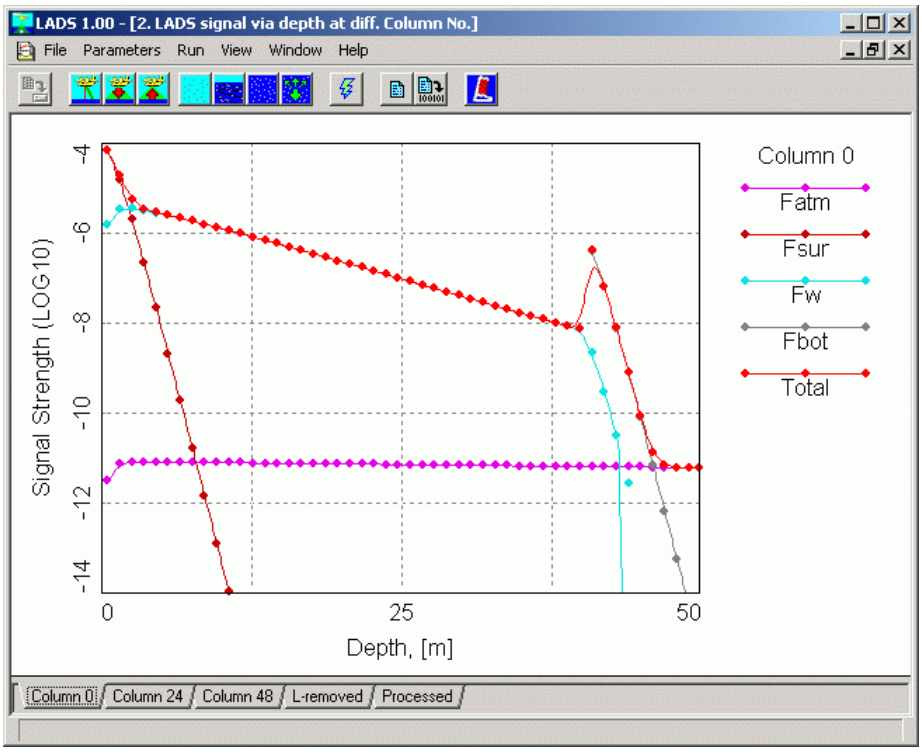

Figure 1: Example of a computer screen for the LADS software with all computed components of the lidar return.

The KSS system parameters as well as the environmental conditions and parameters were entered into the *KSS* model. Weather conditions were clear during lidar data collection; 20 km visibility was used and 10-knot winds for Station 1 and 5-knot winds for Station 5 were recorded and therefore used in the model. For both stations strong optically dense layers existed starting at depths of about 13-15 meters.

In Figure 2 the experimental lidar data (lidar CH1 and lidar CH2 for channels 1 and 2, respectively) are compared with the *KSS* model results (Model CH1 and Model CH2) for Station 1. System noise in the lidar waveform limits comparison at about 15m depth but prior to that point the model data compares exceptionally well with experimental data. For both channels model and lidar data track extremely well to 10 m, where slight slope deviations occur in Channel 1 and system noise dominates Channel 2.

The comparison of model and LIDAR data for Station 5 is shown in Figure 3. The absorption and extinction coefficient profiles for Station 5 show a nearly homogeneous layer in the first 15 meters with much lower average $\langle a \rangle$ and $\langle c \rangle$ values than for Station 1. The KSS LIDAR data and the model data compare extremely well. Again, comparisons are limited at depth due to the system noise. A more detailed description of this comparison is given in (21).

THEORY

The decisive contribution of multiple scattering to the signal return in oceanic lidars is the key issue of the problem. The conventional way to simulate lidar returns with multiple scattering is the use of the Monte Carlo method, but Monte-Carlo modelling of ocean lidar performance takes a lot of time even with powerful computers and for drastically simplified models of media and system.

Another way to compute the lidar return with multiple scattering is to use the small-angle approximation to model the beam propagation. The physical model of the genesis of lidar return takes into account the light multiply scattered to small angles and one time scattered in backward directions

(22). The approach is associated with the fact that the elastic scattering phase functions of seawaters are strongly peaked in the forward direction. As a result, the intensity of scattered light produced by the laser source has a strong peak in this direction. In some particular cases (phase function does not depend on scattering angle near backward direction, co-axial system) this approach provides a fast simulation of the lidar return.

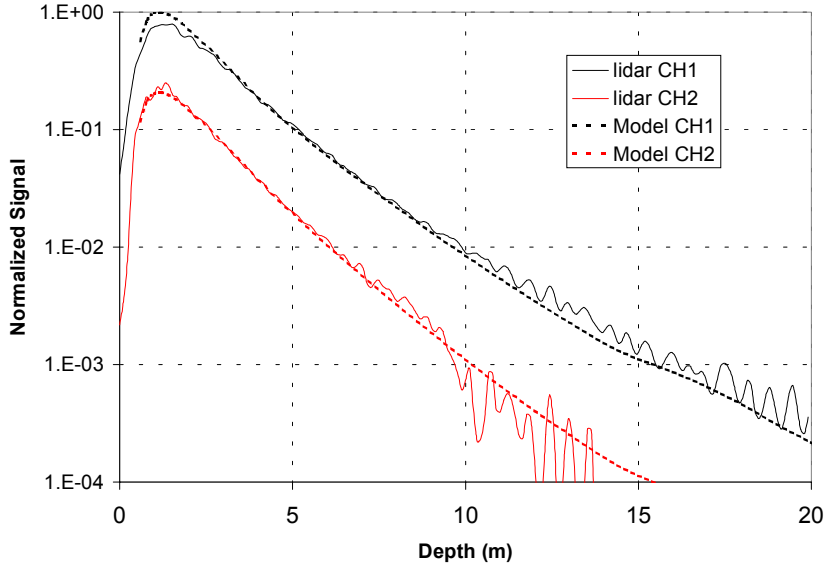

Figure 2: Comparison of the experimental data (lidar CH1 and lidar CH2) and KSS model results (Model CH1 and Model CH2) for Station 1. For the upper ocean water layer of 13 m the average absorption and extinction coefficients are $\langle a \rangle \approx 0.065\, m^{-1}$ *and* $\langle c \rangle \approx 0.4\, m^{-1}$*, respectively.*

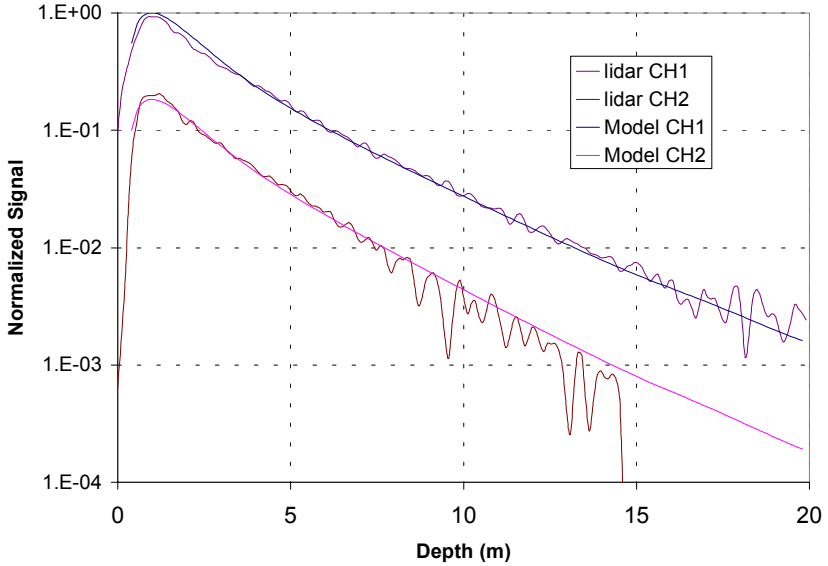

Figure 3: Comparison of the experimental data (lidar CH1 and lidar CH2) and KSS model results (Model CH1 and Model CH2) for Station 1. For the upper ocean water layer of 15 m the average absorption and extinction coefficients are $\langle a \rangle \approx 0.053\, m^{-1}$ *and* $\langle c \rangle \approx 0.18\, m^{-1}$*, respectively.*

The next important step was to develop the specific backscattering technique (7,8) that reduces the problem of backscattering to the much simpler problem of one-way propagation in some effective scattering medium with the IOP defined through the IOP of a real medium and with some effective source. This technique generalizes the approach (22), providing a general solution for any source and receiver patterns, any mutual location of source and receiver, and any phase function. With this technique an analytical relationship between the power of the elastic lidar return $F(z)$, z being a sounding depth, and medium optical characteristics arrives in the form (7,8):

$$F(z) = \mathrm{W}_0 \frac{b_{ef}^b(z)}{4\pi} \frac{v}{2} \int P_{ef}^b\left(\left|\mathbf{n}_\perp\right|\right) I_{ef}(z, \mathbf{r}=0, \mathbf{n}_\perp)\,\mathrm{d}\mathbf{n}_\perp\,, \tag{2}$$

where W_0 is the pulse energy, v, the speed of light in the medium, $b_{ef}^b(z)$ and $P_{ef}^b\left(\left|\mathbf{n}_\perp\right|\right)$ are the scattering coefficient and phase function in the near-backward directions of a certain effective medium, $\left|\mathbf{n}_\perp\right|$, the projection of the unit vector $\mathbf{n}$ onto the plane $z = \text{const}$. The value of $I_{ef}(z, \mathbf{r}, \mathbf{n}_\perp)$ is the light radiance, produced in the point $(z, \mathbf{r})$ of the effective medium by the effective source with a diagram

$$\varphi_{ef}(\mathbf{r}, \mathbf{n}_\perp) = \int \varphi_{src}(\mathbf{r}', \mathbf{n}_\perp') \varphi_{rec}(\mathbf{r}' + \mathbf{r}, \mathbf{n}_\perp' + \mathbf{n}_\perp)\,\mathrm{d}\mathbf{r}'\mathrm{d}\mathbf{n}_\perp'\,. \tag{3}$$

Here $\varphi_{src}(\mathbf{r}, \mathbf{n}_\perp)$ and $\varphi_{rec}(\mathbf{r}, \mathbf{n}_\perp)$ are the spatial-angular patterns of the source and receiver, respectively. Within the small-angle approximation, the Fourier transform of the light radiance $I_{ef}(z, \mathbf{r}, \mathbf{n}_\perp)$ is equal to (15):

$$I_{ef}(z, \mathbf{p}, \mathbf{q}) = \varphi_{ef}(\mathbf{q}, \mathbf{p} + \mathbf{q}z) \exp\left(-\int_0^z \left[c_{ef}(\xi) - \frac{b_{ef}(\xi)}{4\pi} P_{ef}^f\left(\left|\,\mathbf{p} + \mathbf{q}(z-\xi)\,\right|\right) \right] \mathrm{d}\xi \right) \tag{4}$$

where $\varphi_{ef}(\mathbf{p}, \mathbf{q})$ and $P_{ef}^f(\mathbf{p})$ are the Fourier transforms of the effective source diagram $\varphi_{ef}(\mathbf{r}, \mathbf{n}_\perp)$ and of the effective forward phase function $P_{ef}^f(\beta)$, respectively. In this case the properties of the effective medium (the extinction c_{ef}, scattering b_{ef} and b_{ef}^b coefficients, and phase function $P_{ef}(\beta)$) are defined through the IOP of the real medium (c, b and phase function $P(\beta)$) as follows:

$$c_{ef} = 2c, \quad b_{ef} = 2b, \quad b_{ef}^b = b\,, \tag{5}$$

$$\begin{aligned} P_{ef}^f(\beta) &= P(\beta) \qquad \text{at} \quad \beta < \pi/2 \\ P_{ef}^b(\pi - \beta) &= P(\pi - \beta) \quad \text{at} \quad \beta \geq \pi/2 \end{aligned} \tag{6}$$

These IOP of the effective medium for the elastic lidar signal are collected in the first line of Table 1.

Recently this theory was generalized to describe signals from lidars with polarization devices (9), Raman lidar (11), and laser-induced fluorescence.

The theory of the polarized lidar return is entirely based on the new approach to the polarized radiation transfer problem developed in (9,10). As usual, we use the Stokes vector $\mathbf{I}$ to describe polarized radiation in a layer and the four-by-four single scattering matrix $a_{ij}(\beta)$ ($i, j = 1, 2, 3, 4$) (Mueller matrix) with the scattering phase function as its first element ($a_{11}(\beta) = P(\beta)$) to characterize polarization optical properties of a scattering medium. The problem of backscattering of the polarized laser beam completely reduces to the solved scalar problem (the problem without polarization) (9). If we consider for simplicity only the linearly polarized laser pulse, the lidar return can be described by only two Stokes parameters: *I* (radiance without an analyzer) and *Q* (purely linearly polarized light, which is a difference between the signals passing the CO-polarizer and CROSS-polarizer, respectively). The first parameter of the Stokes vector is defined exactly as in the correspondent scalar case by Eqs. (2-6). To get the second Stokes parameter it is enough to use the same Eqs. (2-4) with parameters of the effective medium, given in the second line of Table 1 (see (9)). The effective phase functions in the case are defined via diagonal elements of the seawater Mueller matrix a_{ii}. The semi-empirical model of these elements for seawaters was developed and checked (23).

In seawater, hydrosol particles produce elastic (Mie) scattering, while water molecules are the source of Raman scattering with a wavelength shift in respect to the incident wavelength λ_0.

Table 1: Optical parameters of the effective medium for elastic and non-elastic lidar returns

Problem		b_{ef}^{b}	b_{ef}	c_{ef}	$P_{ef}^{b}(\beta)$	$P_{ef}^{f}(\beta)$
Elastic scattering	First Stokes parameter	b	$2b$	$2c$	$P(\pi-\beta)=a_{11}(\pi-\beta)$ at $\beta \geq \pi/2$	$P(\beta)=a_{11}(\beta)$ at $\beta < \pi/2$
	Second Stokes parameter	b	$2b$	$2c$	$\frac{a_{22}(\pi-\beta)-a_{33}(\pi-\beta)}{2}$	$\frac{a_{22}(\beta)+a_{33}(\beta)}{2}$
Non-elastic processes	Raman	b_R	$b(\lambda_0)+b(\lambda_R)$	$c(\lambda_0)+c(\lambda_R)$	$\frac{3}{4}\Delta_1\left(1+\Delta_2\cos^2\beta\right)$	$\frac{b(\lambda_0)P(\beta,\lambda_0)+b(\lambda_R)P(\beta,\lambda_R)}{b(\lambda_0)+b(\lambda_R)}$
	Fluores-cence	η_F	$b(\lambda_0)+b(\lambda_F)$	$c(\lambda_0)+c(\lambda_F)$	1	$\frac{b(\lambda_0)P(\beta,\lambda_0)+b(\lambda_F)P(\beta,\lambda_F)}{b(\lambda_0)+b(\lambda_F)}$

Our model of the genesis of Raman lidar return is the following. Photons travel from a source into a medium via forward-directed elastic multiple scattering, then a single Raman scattering in a backward direction with a frequency shift, scattering coefficient b_R, and Raman phase function occurs. Photons return from a depth z to the receiver with the elastic multiple scattering in forward directions at a shifted wavelength λ_R. This process is completely analogous to the elastic paradigm and the Raman lidar return is defined by the same structure of solution as in elastic scattering case (Eqs. (2-4)) with the parameters of the effective medium given in the third line of Table 1 (see (11)). The Raman scattering coefficient b_R is a product of molecule concentration by the scattering cross-section of a single molecule. The phase function of the Raman scattering, which defines the backward scattering phase function of the effective medium $P_{ef}^{b}(\beta)$, is the well-known Rayleigh phase function

$$P_{ef}^{b}(\beta)=\frac{3}{4}\Delta_1\left(1+\Delta_2\cos^2\beta\right) \tag{7}$$

with $$\Delta_1=\frac{1+3\rho}{1+2\rho},\ \Delta_2=\frac{1-\rho}{1+3\rho}\ .$$

Here ρ is the depolarization ratio for incident light, linearly polarized perpendicularly to the scattering plane. The effective medium forward phase function $P_{ef}^{f}(\beta)$ is defined through the phase function $P(\beta)$ and scattering coefficients of the real medium at an incident wavelength λ_0 and a shifted wavelength λ_R, as defined in the Table 1.

As seen, the problem of Raman backscattering is completely reduced to the solved elastic problem (see in more detail (11)).

The temporal dependence of laser-induced fluorescence can be obtained with the model analogous to the model of the genesis of Raman lidar signal. The incident light with the wavelength λ_0 propagates from a laser into a medium with small-angle multiple scattering. Then an act of fluorescence occurs (absorption of the incident photons and emittance of the fluorescence photons with the wavelength λ_F and the isotropic angular diagram). These fluorescence photons return from the depth z to the receiver with the elastic multiple scattering in forward directions at a shifted wavelength λ_F. It means that power of the laser-induced fluorescence is given by Eqs. (2-4) with the effective medium parameters defined in the last line of Table 1. η_F is a parameter proportional to the product of a quantum efficiency of fluorescence and the fluorophore concentration. Since the fluorescence has an isotropic angular pattern, the backward effective medium phase function $P_{ef}^{b}(\beta)=1$. The extinction and scattering coefficients of the effective medium as well as the forward

phase function $P_{ef}^{f}(\beta)$ are formed completely analogous to the case of Raman lidar return through parameters of the real medium at the initial and fluorescence wavelengths (see Table 1).

With the developed technique computations of polarized elastic and Raman lidar returns as well as laser-induced fluorescence take a few seconds on PC versus hours with large computers with the most advanced Monte Carlo algorithms. The excellent coincidence of the model with Monte-Carlo simulations was demonstrated in (9) and (24).

The above general theory provides a good basis for developing high-speed efficient algorithms to simulate lidar performance. To provide quasi real-time accurate simulations, analytical models of the axis irradiance and axis intensity should meet at least two requirements: they should take into account the inherent singularity of the point spread function and allow the analytical integration for multi-dimensional integrals, which arrive in a simulation algorithm. Even the most advanced recently developed models of the beam spread function (BSF) (25,26) failed to meet the above two requirements. We have developed the new beam spread function model, which not only meets these requirements but, unlike the small-angle solution, allows a description of the forward pulse stretching and remains accurate for comparatively large depths (24).

A laser sounding theory usually ignores the pulse stretching for the reason that it is small enough in comparison with the spread of the backscattering pulse. Nevertheless, there exist situations, particularly laser sounding of deep waters or seabed ranging, where the allowance for the temporal forward pulse stretching cannot be neglected (see examples in (24)). Using the new BSF model, we have developed an approach to describe the forward pulse stretching. The simple recipe how to compute the mean time and variance in the case of stratified seawater has been elaborated and briefly described in (24).

Inversion of elastic and Raman lidar returns

The developed fast simulation is a key to the inverse problem solution and developing retrieval techniques. Although some inversion approaches have been already developed (27-30), the reliable techniques for waveforms inversion and for retrieval the IOPs profiles are lacking at present.

The most important recent result is an analytical inversion of the elastic lidar equation with multiple scattering in the common case without any prior suggestions on the seawater optical properties.

Equ. (2) with regard to $b_{ef}^{b}(z) = b(z)$ can be rewritten in the form

$$F(z) = b(z)E(z) \tag{8}$$

where

$$E(z) = \frac{W_0}{4\pi}\frac{v}{2}\int P_{ef}^{b}\left(|\mathbf{n}_{\perp}|\right) I_{ef}(z, \mathbf{r}=0, \mathbf{n}_{\perp})\,\mathrm{d}\mathbf{n}_{\perp}\,. \tag{9}$$

Introducing the logarithmic derivative of the function $E(z)$

$$g(z) = -\frac{d\left[\ln E(z)\right]}{dz} = -\frac{1}{E(z)}\frac{dE(z)}{dz}, \tag{10}$$

we get:

$$F(z) + \frac{b(z)}{g(z)}\frac{dE(z)}{dz} = 0\,. \tag{11}$$

A solution of Equ. (11) with regard to Equ.(8) is

$$E(z) = \frac{F(z_0)}{b(z_0)} + \int_{z}^{z_0}\frac{F(z')}{b(z')}g(z')dz'\,. \tag{12}$$

From Eqs. (8) and (12) one obtains:

$$b(z) = b(z_0)\frac{F(z)}{F(z_0) + b(z_0)\int_z^{z_0} F(z')B(z')dz'}, \tag{13}$$

$$B(z) = \frac{g(z)}{b(z)} = -\frac{1}{b(z)}\frac{d\left[\ln E(z)\right]}{dz}. \tag{14}$$

The simple solution (13) implies only one wide-used assumption: it takes into account only photons one time scattered onto large angles. It is important that Equ. (13) includes all already known solutions of the lidar equation as the particular cases. It works under single and multiple scattering, for any geometry (the narrow and wide beams cases), for any set of the medium inherent optical characteristics dependent on depth, and for any reference point in the retrieval procedure. Particularly, for the single scattering in atmosphere, when absorption can be neglected and $c(z) = b(z)$, one has:

$$g(z) = 2b(z), \qquad B(z) = 2\ , \tag{15}$$

and solution (13) passes to the well-known form

$$b(z) = b(z_0)\frac{F(z)}{F(z_0) + 2b(z_0)\int_z^{z_0} F(z')dz'}. \tag{16}$$

If the choice of the reference point is $z_0 = 0$, Equ. (16) passes into the solution published in (31). If the reference point z_0 is chosen at the remote end of the sounding path, Equ. (13) coincides with the known Klett solution (see (32)). Equ. (14) defines the well-known empirical Platt correction factor, which was introduced to allow for the multiple scattering (33). It was supposed that this factor should be specified from Monte Carlo computation data.

We developed a retrieval algorithm based on Equ. (13). The iteration procedure requires multiple computations of lidar return with different IOPs profile and in this process our modelling looks indispensable.

Figures 4 and 5 give an example of the lidar waveform and the results of its inversion with solution (13) and iteration performed with AOLS in comparison with the sea truth. This inversion technique is brand-new and various particular implementations are actually under development.

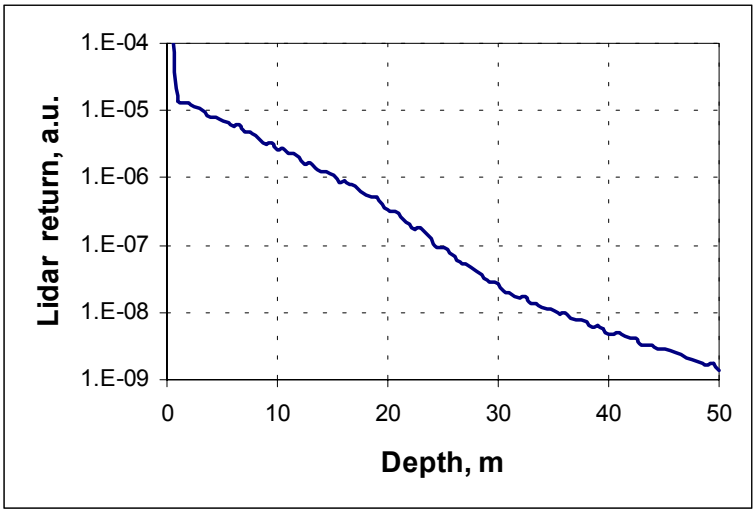

Figure 4: Lidar return in the LADS system.

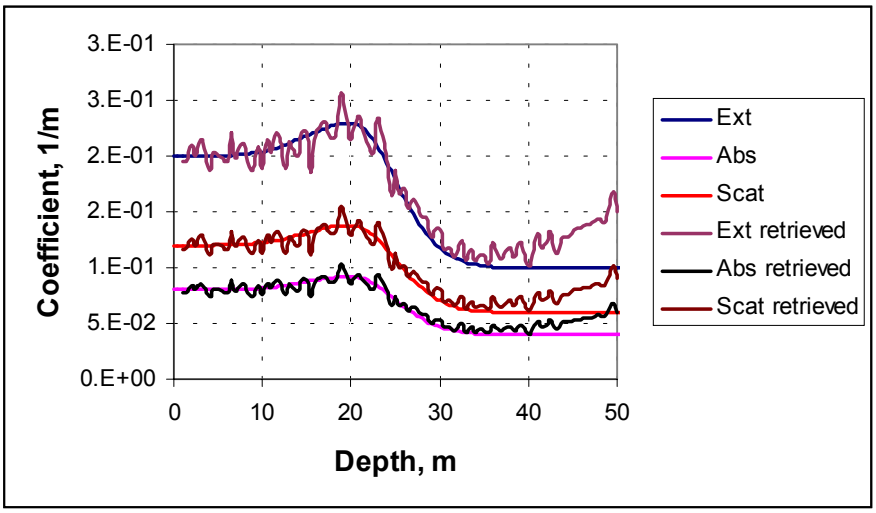

Figure 5: An example of retrieval of the extinction (Ext retrieved), absorption (Abs retrieved), and scattering (Scat retrieved) coefficients from the lidar return in LADS system (see Figure 4) in comparison with sea truth.

The use of the Raman channel is a standard technique to investigate seawater properties by lidar sounding (34). The known Raman scattering phase function allows troubles with the near-backward scattering in seawaters to be avoided and the depth-independent Raman scattering coefficient may be used as a reference signal for other (e.g., fluorescence) measurements.

Recently we suggested a new technique for measuring seawater-backscattering profiles by a new combined Raman-elastic lidar with different initial wavelengths particularly specified (34). It allows the Raman channel to be used as a reference without exact a priori knowledge of sounding medium spectral characteristics and properly regards multiple scattering. An example of the retrieval of the scattering profile with this technique is depicted in Figure 6 (for more details see (34)).

The joint use of Raman, fluorescence, and elastic lidar returns, including polarization characteristics can significantly enlarge the retrieval capabilities of ocean lidars. The developed solution and AOLS modelling provide a basis for further development in this direction.

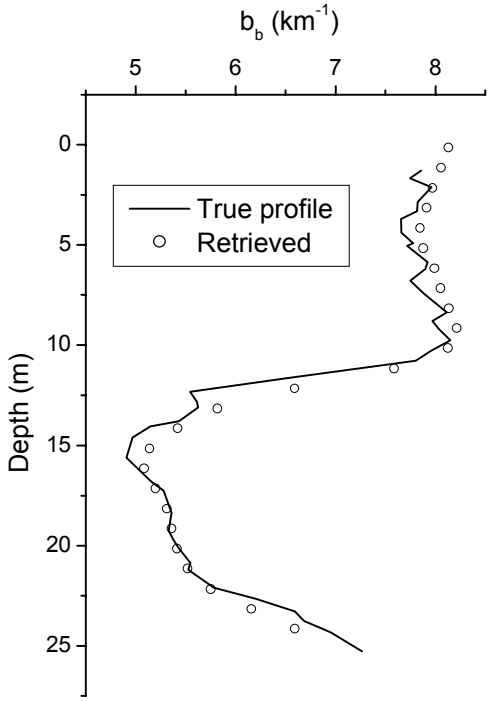

Figure 6: Example of the retrieval of the scattering profile with combined Raman-elastic lidar.

CONCLUSIONS

1. The family AOL software, which simulates the performance of the airborne ocean lidars in quasi real-time, is outlined. This modeling estimates the lidar return signal and its components due to the atmosphere, atmosphere-ocean interface, seawater, and bottom in various regions of the world's oceans with specific water stratification and at any bottom level, in daylight and at night under different weather conditions.

2. A successful comparison of experimental and modeled lidar data is performed, using a unique opportunity provided by the HyCODE 2001 field test, where KSS lidar profiles and near simultaneous in situ IOP profiles were collected off the coast of New Jersey.

3. A general analytical theory is briefed that describes elastic and Raman lidar returns and laser-induced fluorescence with polarization and multiple scattering, and serves as a core of the simulating algorithm.

4. First advances in the inversion of the lidar waveforms on the basis of the new common solution of the lidar equation with multiple scattering and the developed fast simulation technique are outlined. We have discussed here only the very first steps in the technique for the inversion of the oceanic lidar profiles. Currently this technique is under development in our group and the progress looks impressive. We would like to underline that just fast and accurate computer modeling of the lidar returns is a core of our inversion procedures.

ACKNOWLEDGMENTS

The authors are grateful to Dr. L. I. Chaikovskaya who participated in developing the theory of polarized lidar returns.

This work was supported by the ISTC Project #B-519p.

REFERENCES

1 Hickman G D & J E Hogg, 1969. Application of an airborne pulsed laser for near-shore bathymetric measurements, Remote Sensing of Environment, 1: 47-58

2 Ivanov, A P, A L Skrelin & I D Sherbaf, 1972. Study of optical characteristics of water media using pulsed sounding. Journal of Applied Spectroscopy (USSR), 17: 232-240

3 Guenther G C, A G Cunningham, P E LaRocque & D J Reid, 2001. Meeting the accuracy challenge in airborne lidar bathymetry. EARSeL eProceedings, 1(1): 1-27

4 Alloca D, V M Contarino & B Concannon, 1998. Remote sensing of the ocean using the airborne KSS lidar. In: Ocean Optics XIV, CD-ROM (Office of Naval Research, Washington, D.C.)

5 Gordon H R, 1982. Interpretation of airborne oceanic lidar: effects of multiple scattering. Applied Optics, 21: 2996-3001

6 Harsdorf S & R Reuter, 1999. Laser remote sensing of sunken chemicals in highly turbid waters: validity of the lidar equation. In: Environmental Sensing and Applications. Proceedings EUROPTO Series, SPIE 3821, 369-377

7 Zege E P, I L Katsev & I N Polonsky, 1995. Analytical solution to lidar return signals from clouds with regard to multiple scattering. Applied Physics, B60: 345-353.

8 Katsev I L, E P Zege, A S Prikhach & I N Polonsky, 1997. Efficient technique to determine backscattered light power for various atmospheric and oceanic sounding and imaging systems. Journal of Optical Society of America A, 14: 1338-1346

9 Zege E P & L I Chaikovskaya, 1999. Polarization of multiple scattering lidar return from clouds and ocean water. Journal of Optical Society of America A, 16: 1430-1438

10 Zege E P & L I Chaikovskaya, 2000. Approximation theory of linearly polarized light propagation through the scattering medium. Journal of Quantity Spectroscopy and Radiative Transfer, 66: 413-435

11 Malinka A V & E P Zege, 2003. Analytical modeling of the Raman lidar return including multiple scattering. Applied Optics, 24: 1075-1081

12 Casey M J, 1984. Deploying the lidar on hydrographic surveys. Proceedings of the 9th Canadian Symposium on Remote Sensing, Memorial University, 165-175

13 Australian Laser Airborne Depth Sounder, LADS Corporation

14 Walker R E, 1994. Marine Light Field Statistics (Wiley, New York) 675 pp.

15 Zege E P, A P Ivanov & I L Katsev, 1991. Image Transfer through a Scattering Medium (Springer Verlag, Heidelberg)

16 Dreischuh T N, L L Gurdev & D V Stoyanov, 1995. Effect of pulse-shape uncertainty on the accuracy of deconvolved lidar profiles. Journal of Optical Society of America A., 12(2): 301-306

17 Harsdorf S & R Reuter, 2001. Stable deconvolution of noisy lidar signals. EARSeL eProceedings, 1(1), 88-95

18 Park Y J, S W Dho & H J Kong, 1997. Deconvolution of long-pulse lidar signals with matrix formulation. Applied Optics, 36: 5158-5161

19 Guenther G C, 1986. Wind and nadir angle effects on airborne lidar water surface returns. In: Ocean Optics VIII, SPIE 637: 277-286

20 Guenther G C & R W L Thomas, 1984. Effects of Propagation-induced Pulse Stretching in Airborne Laser Hydrography. In: Ocean Optics VII, SPIE 489: 287-296

21 Concannon B M, E P Zege, D Allocca, T Curran, J Prentice, I L Katsev & A S Prikhach, 2003. Experimental and modeled lidar data can agree in the real world. In: II International Conference Current Problems in Optics of Natural Waters, edited by I. Levin & G. Gilbert (St.-Petersburg) 119-124

22 Dolin L S & V A Savel'ev, 1971. Characterization of back scattering signal at pulse radiation of turbid medium by a narrow directional light beam. Izvestiya of Academy of Sciences of USSR, Atmospheric and Oceanic Physics, 7: 505-510

23 Zege E P, I L Katsev & A S Prikhach, 2001. Simulation of the performance of ocean imaging lidar with polarization devices. In: International Conference Current Problems in Optics of Natural Waters, edited by I Levin & G Gilbert (St.-Petersburg) 32-38

24 Zege E P, I L Katsev, A S Prikhach, G D Ludbrook & P Bruscaglioni, 2002. Analytical and computer modeling of the ocean lidar performance. In: 12th International Workshop on Lidar Multiple Scattering Experiments (MUSCLE-12), SPIE 5059: 189-199

25 Dolin L S & V A Savel'ev, 2000. New model for the light-beam spread function in a medium with strongly anisotropic scattering. Izvestiya of Academy of Sciences of USSR, Atmospheric and Oceanic Physics, 36: 794-801

26 McLean J W, J D Freeman & R. E. Walker, 1998. Beam spread function with time dispersion. Applied Optics, 37: 4701-4711

27 Goldin Y A, A P Vasilkov, B A Gureev, F E Hoge, R N Swift & C W Wright, 2001. Airborne polarization lidar observation of 2D spatial structure of near-bottom scattering layers. In: International Conference Current Problems in Optics of Natural Waters, edited by I Levin & G Gilbert (St.-Petersburg) 127-132

28 Bissonette L & R Gilles, 2000. Retrieval of cloud liquid water content and effective droplet diameter from multiply scattered lidar returns. Proceedings of the 20th ILRS (Vichy, France) 251-254

29 Veretennikov V V, G P Kokhanenko & V S Shamanaev, 2000. Interpretation of the data of seawater lidar sensing. Proceedings of the 20th ILRS (Vichy, France) 145-148

30 Feygels V I, Y I Kopilevich, A Surkov, J K Yungel & M J Behrenfeld, 2003. Airborne lidar system with variable field-of-view receiver for water optical properties measurement. In: Ocean Remote Sensing and Imaging II. SPIE, 5155: 12-21

31 Zege E P, A P Ivanov, I L Katsev, B A Kargin & G A Mikhailov, 1971. Determination of the extinction and absorption coefficients of sea water and atmosphere through reflected pulse spread. Izvestiya of Academy of Sciences of USSR, Atmospheric and Oceanic Physics, 7: 750-757

32 Klett J, 1986. Extinction boundary value algorithms for lidar inversion. Applied Optics, 25: 2462-2464

33 Platt C M R, 1973. Lidar and radiometric observations of cirrus clouds. Journal of Atmospheric Sciences, 30: 1191-1204

34 Malinka A V & E P Zege, (in press). New technique to retrieve the seawater backscattering profiles from coupling Raman and elastic lidar data. Applied Optics